www.elsevier.com/locate/memsci

Fabrication of thin film composite poly(amide)-carbon-nanotube supported membranes for enhanced performance in osmotically driven desalination systems

Ludovic Dumée, Judy Lee, Kallista Sears, Blaise Tardy, Mikel Duke, Stephen Gray

PII: S0376-7388(12)00697-7
DOI: http://dx.doi.org/10.1016/j.memsci.2012.09.026
Reference: MEMSCI11631

To appear in: *Journal of Membrane Science*

Received date: 19 April 2012
Revised date: 3 September 2012
Accepted date: 16 September 2012

Cite this article as: Ludovic Dumée, Judy Lee, Kallista Sears, Blaise Tardy, Mikel Duke and Stephen Gray, Fabrication of thin film composite poly(amide)-carbon-nanotube supported membranes for enhanced performance in osmotically driven desalination systems, *Journal of Membrane Science,* http://dx.doi.org/10.1016/j.memsci.2012.09.026

Fabrication of thin film composite poly(amide)-carbon-nanotube supported membranes for enhanced performance in osmotically driven desalination systems

Ludovic Dumée[1*#], Judy Lee[1*], Kallista Sears[2], Blaise Tardy[1], Mikel Duke[3], Stephen Gray[4]

[1.] Department of Chemical and Biomolecular Engineering, The University of Melbourne, Parkville, Victoria 3010, Australia

[2.] CSIRO, Materials Science and Engineering, Clayton South, Victoria 3169, Australia

[3.] School of Engineering and Science at Victoria University, Werribee, Victoria, 8001, Australia

[4.] Institute for Sustainability and Innovation at Victoria University, Werribee, Victoria 8001, Australia

[#] corresponding author – ludo.dumee@hotmail.com ; phone: +61410131312

* these two authors equally contributed to the manuscript

Abstract

The search for lower energy consumption desalination systems has been driving research in the past decade towards the investigation of osmotically driven membrane processes, such as forward osmosis (FO) or osmotic distillation (OD). Despite similarities with reverse osmosis (RO) membranes, thin film composite (TFC) for FO membranes require careful design to reduce salt concentration polarization formation within the large pores composing the supporting layer. An investigation of a novel, highly stable, robust support made solely of carbon nanotubes (CNTs), which could find applications in both RO and FO was undertaken. TFC membranes were fabricated by interfacially polymerizing for the first time a dense poly(amide) (PA) layer on self-supporting bucky-papers (BPs) made of hydroxyl-functionalized entangled CNTs. These hydrophilic supports exhibited low contact angle with water (< 20^{o}), high water uptake capacity (17 wt%), large porosity (> 90%), making it a promising material when compared with poly(sulfone) (PSf), the traditional polymer used to fabricate TFC membrane supports in RO. In addition, the impact of the support hydrophilicity on the stability of the interfacially polymerized film and on water adsorption was investigated by oxygen-plasma treating various potential support materials, exhibiting similar geometrical properties. The morphology and salt diffusion of both CNT BP and PSf supports were investigated, and the novel BP-PA composite membranes were found to be superior to commercially available TFC membranes.

Keywords

Carbon nanotube bucky-paper; forward osmosis; thin film composite membrane; poly(amide) interfacial polymerization

1. Introduction

Reverse osmosis (RO) dominates today's global desalination market as it offers several advantages over thermally or electrically driven desalination techniques including being less energy demanding and more robust for large desalination projects [1, 2]. However, since the late 90's the quest for more energy efficient technologies have pushed research in the direction of osmotically driven desalination techniques such as forward osmosis (FO) [3, 4]. FO has shown promise when integrated along with membrane bio-reactors [5], nano-filtration [6] or membrane distillation [7] in order to reduce organic fouling [8] when treating highly concentrated organic solutions or RO brines. Although the operating principles of RO and FO highly differ from each other, the first membranes designed for FO were very similar to RO membranes [9, 10]. Similarities in the required salt rejection and properties of the thin active layer of the membranes initially lead research on FO towards using the expertise on RO membrane fabrication to process FO membranes [11, 12]. However, the different operational principles dictated that an alternative structure could lead to better performance in FO. Water permeation in RO relies on external applied pressure to overcome the osmotic pressure difference across a dense water soluble membrane to force water from the concentrate feed to the dilute permeate [13], while FO operates on the basis of exploiting the osmotic pressure difference to drive water across the dense layer of a semi-permeable membrane from a dilute feed into a concentrated draw solution. In both the RO and FO systems, the porous membrane supports have a significant effect on the efficiency of the application of interest but have generally been neglected in the research literature [4, 14].

Molecular transport in a water soluble polymer membrane is assumed to follow the solution-diffusion model [15] where the membrane's thin active layer undertakes the functional separation. It is often assumed that the diffusional resistance across the porous sub-layer is very low and that the transport properties of the membrane are determined only by the active layer. However, studies on asymmetric cellulose acetate membranes in RO have shown that the concentration gradient in the porous sub-layer can be significant, comprising up to 22 % of the total resistance of the membrane [16,

17]. Similarly, in the case of FO, recent investigations demonstrated that the porosity and thickness of the macro porous support layer [18, 19] were likely to influence the membrane resistance to salt diffusion [3] due to the formation of large boundary layers within the support layer [15, 20]. While FO has the advantage of being less affected by pressure based fouling (i.e. cake formation) since no high pressure is applied on the membrane surface, it was demonstrated to be more sensitive to internal concentration polarization (ICP) than RO. ICP generated within the supports affect performance and well-engineered membranes are required to reduce permeation decay and improve the process efficiency [21]. ICP in the porous sub-layer of asymmetric cellulose acetate membranes have for instance been demonstrated to be significant [16, 17]. Large performance losses were demonstrated to occur when inappropriate membranes, such as commercial RO membranes [9, 22, 23], were used in FO. An optimal FO membrane support was previously described as thin, highly porous, of low tortuosity and strongly hydrophilic [24, 25]. The reduction of external concentration polarization has been investigated in both RO and FO through the use of specifically designed module spacers [26, 27], the better design of membrane structure [26] and chemical functionalization of membrane surface in order to change the membranes surface wetting behavior [15].

A number of fabrication strategies have been developed to increase the average membrane permeability while maintaining high salt rejection, but more work is clearly needed to develop membranes specifically designed for FO. To date, although some asymmetric membranes were shown to exhibit high performance, thin film composite (TFC) membranes have dominated the commercial RO markets due to their lower fabrication costs and higher stability regardless of the feed quality and composition. Although, these supports exhibit poor wetting properties [25] and strong internal concentration polarization [4, 24, 28], they are the dominant material in the field of RO desalination technology, valued for their high water fluxes and salt rejection, and good tolerance to large pH variations. TFC membranes are composed of a thin top active layer supported on a macro-porous layer. The thickness of this top layer may vary but is usually between 100 and 500 nm [2]. An extensive number of studies have focused on

improving the selective layer by investigating more water permeable polymers and composite nano-structures [29]. Very little attention has, however, been focused on the optimization of both the FO and RO membrane supporting layers and typical supports for TFC membranes are non-woven poly(ester) and poly(sulfone) (PSf) [1, 20]. To date, the only commercial FO membranes available on the market are asymmetric membranes from Hydration Technologies Inc. (HTI, Albany OR – USA), based on cellulose triacetate embedded into a woven polyester mesh [30] and membranes from Modern Water. Improvements of the support structure would therefore improve the permeability of current TFC membranes [14, 29] and possibly make them better candidates for FO.

A few studies have focused on the development of new supports for RO [31] and FO [18] membranes but, to the best of our knowledge, the impact of the support thickness, porosity or compressibility on the permeation process is always assumed to be predominantly ruled by the selective top layer. Yang et al. first demonstrated the importance of the porosity and structure of the support layer when testing hollow fiber membranes in FO initially prepared for nano-filtration [32]. Furthermore, Wei et al. [33] prepared PSf supports by phase inversion, which exhibited long finger-shaped cavities and porosities between 77 and 81 %. These supports had geometrical S coefficients between 0.67 and 0.71 mm making them comparable with commercial membranes from HTI (Table 1). Recent work on novel supports successfully used an electro-spun nanofibre mesh as a template for ICP [34]. Amongst other promising candidates to improve the performance of FO and RO membranes, carbon nanotubes (CNTs) show outstanding properties that could lead to more robust and flexible [35], chemically resistant supports [36] that may be less susceptible to ICP. CNTs can be organized in a variety of macro-structures, either self-supporting [37] with no binding materials and using Van der Waals forces to hold the CNTs together [38], as parallel arrays of CNTs, after collapsing aligned CNT forest by solvent evaporation [39] or through a composite approach by integrating the CNTs within a mixed matrix structure [40]. Furthermore, although the price of pristine CNTs was an obstacle over the past decade to their large scale commercialization, its cost has been reduced continuously and they stand as

promising building blocks in a number of tomorrow's industrial applications [41]. Given the flexibility [42, 43] and large mechanical stiffness of Bucky-papers (BPs), with tensile moduli demonstrated to reach up to 1GPa [37], a non-woven network of entangled CNTs, they have been specifically of interest in the separation [44] and desalination [45] industries. BP can be cheaply processed from any grade of CNTs into very thin layers (> 10 μm) and have been shown to exhibit very large porosities [37, 46]. Furthermore, CNTs can be functionalized in order to fine tune their outer wall surface chemistry and super hydrophilic CNTs BPs have been processed for a large number of applications [47, 48]. Additionally, use of binders within the BP structure could be used to stiffen the BP without significantly affecting overall porosity [45]. Although the high compressibility of BPs without binders [35] could be a limitation to their use as RO supports, the low trans-membrane pressure applied in FO makes them promising candidate structures for current polymeric supports.

In this paper we investigate the role of the structure of the support on the permeation of salt through TFC membranes, fabricated by interfacial polymerization of a poly(amide) (PA) layer on top of a self-supporting, super porous CNT non-woven BP material. Coating CNT BPs with a dense stable polymer film is a novel approach to fabricate ultra-thin membranes and has not been reported in the literature to the best of the authors' knowledge. These promising thin supported structures were characterized prior to testing salt and water diffusion in a diffusion cell. The results were compared to the results for a commercial PSf support.

2. Experimental details

2.1 Chemical reagents and commercial membranes

N,N-dimethyl formamide (DMF) (98 %, Chemsupply), 1,3-phenylenediamine (MPD) (99+%, Aldrich), trimesoyl chloride (TMC) (98 %, Aldrich), sodium chloride (NaCl) (99 %, Chemsupply) and n-hexane (95 %, BDH) were used as received. All solutions were made using Milli-Q water with a resistivity of 18.2 MΩ cm. A commercial poly(amide) membrane, Dow Filmtec BW30LE, and a porous PSf proprietary polymer membrane support were kindly supplied by Dow Filmtec and GE Water, respectively.

2.2 Composite membrane fabrication

Multi-walled CNTs grown by chemical vapour deposition on silicon wafers at the CSIRO Materials Science and Engineering, Clayton, Australia, were used as stock material [49]. The CNTs were first scraped from their growth support wafers and suspended by repeated sonication in propan-2-ol at -17 ^{o}C following a procedure detailed in [45]. The suspensions were then filtered under house vacuum onto commercial 200 nm pore size poly(ether-sulphone) (PES) membranes from Millipore. The BPs were then peeled from the PES membranes to form a self-supporting membrane to act as a support during composite membrane processing. The surface of the CNT BPs was plasma treated with a 10W low pressure oxygen plasma cleaning device in order to render their surface hydrophilic. Both sides of the samples were exposed in a closed chamber at 500 mTorr for 5 min to the plasma. The BP supports were immediately immersed and stored in ethanol after exposure to protect the functional groups formed on the CNTs outer surface. The plasma treatment step was necessary to ensure wetting of the solutions during interfacial polymerization.

The plasma treated BPs were then dried at 50 ^{o}C in an oven prior to be carefully placed over a Whatman filter paper (grade 602h) into a Buchner funnel. A 2 % w/v MPD aqueous solution was poured over the BP to fully cover the membrane and vacuum was

applied to filter the MPD solution through the BP until a thin layer remained. This layer was then drained and the 0.1 % w/v TMC in hexane was carefully poured over the BP and reacted for 10 seconds. Excess organic solution was drained and the BP washed with hexane to remove any unreacted TMC, followed by rinsing with ethanol and water. The BP-PA deposited membranes were then stored in Milli-Q water.

2.3 Commercial membrane supports: PSf and poly(tetra-fluoroethylene)

The porous membrane support provided by GE consisted of polyester and PSf support without the PA active layer. The polyester paper backing was peeled away to give only a single layer of PSf support. This support was used as the supporting layer to perform IP as previously described, except that no vacuum was applied during IP. For the commercial BW30LE membrane, the paper backing was peeled off before testing in the diffusion cell. In addition, IP on top layer of 20 nm pore size poly(tetra-fluoroethylene) (PTFE) membranes from PALL was also performed to compare with the other types of supports. This PTFE support was chosen as it exhibited similar geometrical properties as the PSf and BP supports and provided convenient material to benchmark against the novel BP supported membranes.

2.4 Membrane characterization and salt diffusion tests

The thickness of the membranes was measured using a micrometer (Kincrome digital micrometer). Three measurements at random positions on the sample surface were averaged. The accuracy of the measurement was demonstrated in a previous paper [37], while the porosity of the BPs was also estimated following results on the same CNT structures from previous work.

The membrane supports pore size distribution was determined by perm-porometry with a PMI 1500 capillary flow porometer (CSIRO Materials Science and Engineering, Victoria – Australia). The tests were setup inn a wet/up dry/up mode. Galwick was used as the wetting liquid and 99.99% pure N_2 used as pressurizing

gas. The pressure was incremented by 0.05 PSI per second from 150 PSI up to 450 PSI and the pore size distribution was determined following a procedure previously detailed in [50].

The sorption of water vapour on the membranes was determined using a Gravimetric Sorption Analyzer (GHP-FS, with a Cahn D-200 balance, VTI Scientific Insturments, Florida) in flow mode. Membrane samples were placed in a sample holder that was suspended inside a temperature controlled chamber. The relative humidity (RH) inside the chamber was controlled by varying the flow of saturated and dry helium gas. For a given RH, the system was allowed to equilibrate until a constant mass was recorded. The RH can be related to the activity of water (a_w) [51]:

$$a_w = \frac{RH}{100} = \frac{P_w}{P_{sat}} \qquad (1)$$

Where P_w and P_{sat} are the water vapour partial pressure and the saturated water vapour pressure, respectively.

The relative weight of water adsorbed was calculated using Equation 2:

$$RW(\%) = 100.\frac{(m_{RH} - m_0)}{m_0} \qquad (2)$$

Where m_{RH} is the mass of the sample at a given RH and m_0 the mass of the dry sample, respectively.

The surface structure of aromatic PA films and BPs were imaged using a Philips XL30 FEG FE Scanning Electron Microscope (SEM) at 2kV. All samples were sputter-coated with gold under vacuum prior to imaging. Cross sections of the commercial membranes were prepared by snapping the samples in liquid nitrogen prior to gold sputtering. Furthermore, the cross sections of the BPs were obtained by ion beam milling (Gallium) on a FEI Nova dual beam (at Bio21, Melbourne – Australia).

The membrane and support were compacted under water in a dead end filtration cell at 6.9 MPa and filtered with water to ensure any trapped air was removed and the membranes were fully hydrated. A diffusion cell from Permgear (Figure 1) was used to perform direct osmosis experiments. It consisted of a two compartment cell design. The membrane was sandwiched between two Teflon gaskets and clamped between the two compartments. One compartment (receiver cell) was filled with Milli-Q water whereas the other compartment (donor cell) was filled with 2 g/L NaCl electrolyte solution. The solutions in the two compartments were stirred to reduce external concentration polarization. A water cooling jacket was used to maintain the temperature of the solutions at 25 ^{o}C. The concentration of electrolyte in the receiver cell was recorded as a function of time using a conductivity probe, and the conductivity converted to salt concentration via a calibration curve.

The mass transfer coefficient or flux constant was calculated using Equation 3 [52]:

$$-\frac{V}{2A} ln\left(1-\frac{2C_R(t)}{C_D(0)}\right) = Bt \qquad (3)$$

Where $C_R(t)$ is the salt concentration in the receiver cell at time t, $C_D(0)$ is the initial salt concentration in the donor cell, V is the volume of solution in each cell, *and* A is the membrane area.

In addition, S, the structural parameter, is defined as the product of the support layer thickness (l) and tortuosity (τ) over its porosity (ε) [33] and provides an indication of the diffusion path length across the membrane.

Contact angle measurements were performed with a contact angle goniometer and analysed using CXImage 2.0 software with 5 µL drops of Milli-Q water. Three tests were performed and averaged for each sample. Membrane surface morphology and quantitative surface roughness analysis were performed using a Dimension 3100 Atomic Force Microscope (AFM) (Digital Instruments, Santa Barbara, CA) in tapping mode with a non-coated silicon cantilever at a resonance frequency of 300 kHz using an

AFM probe of force constant 40 N/m. Dry membrane samples were mounted on a specimen holder and a height image of 10 μm x 10 μm area was scanned for 512 samples (giving an average sample length of approximately 19.5 nm). Surface roughness for a 2.5 x 2.5 μm area was reported in terms of the root mean square (RMS) values.

3. Results and discussion

3.1 Membrane supports without aromatic poly(amide) film

The structure of the membrane support is critical to achieving high performance in both FO and RO. The membrane support's wetting by water is especially important as water is one of the co-solvents typically used during interfacial polymerization [25] and is required to permeate rapidly through the membrane during desalination. It is well known that plasma treatment leads to formation of functional 'defect' groups [53]. In this work, the measure of the effectiveness of plasma to impart the essential hydrophilic property is carried out by contact angle. Wetting of the BPs and PSf support surfaces was evaluated by direct contact angle measurements. The contact angle on the BPs was shown to clearly decrease from 115^{o} (± 3 ^{o}) to < 20^{o} (± 3 ^{o}) after plasma exposure while the contact angle on the PSf was found to be 68^{o} (± 2 ^{o}) (Table 1). This demonstrates that the plasma treatment significantly improved the wettability of the BPs by grafting hydroxyl and carboxylic groups on the surface of the CNTs as previously reported [54].

However, surface contact angle does not truly reflect the wetting properties of the bulk of the structure, especially inside the pores where water transport takes place. Therefore water vapour sorption tests were performed on the samples. The water uptake by the BP and PSf supports as a function of relative humidity is shown in Figure 2 a. The plasma exposed BPs showed a significantly higher water uptake of approximately 17.6 ± 1.3 wt % at 95 % RH compared with only 2.55 ± 0.03 wt% for the PSf at the same RH (Table 1). Water sorption by the PSf is via hydrogen bonding between the hydrogen atoms of the water molecule and that of the oxygen of the PSf sulfonyl group [31] and was comparable to that of the non-plasma exposed BPs. In comparison, the plasma exposed BP water uptake was comparable to the 21.5 ± 0.9 wt % by the isolated PA layer. In addition, the thickness of the two supports was quite different as the BPs and PSf supports exhibited thickness of ≈ 12.33 μm (± 1.52 μm) and ≈ 43 μm (± 2.64 μm), respectively. The use of a support that is both highly hydrophilic and thin will in theory allow water to permeate through the support with

reduced resistance. The surface of the supports and their apparent roughness were characterized by AFM as shown in

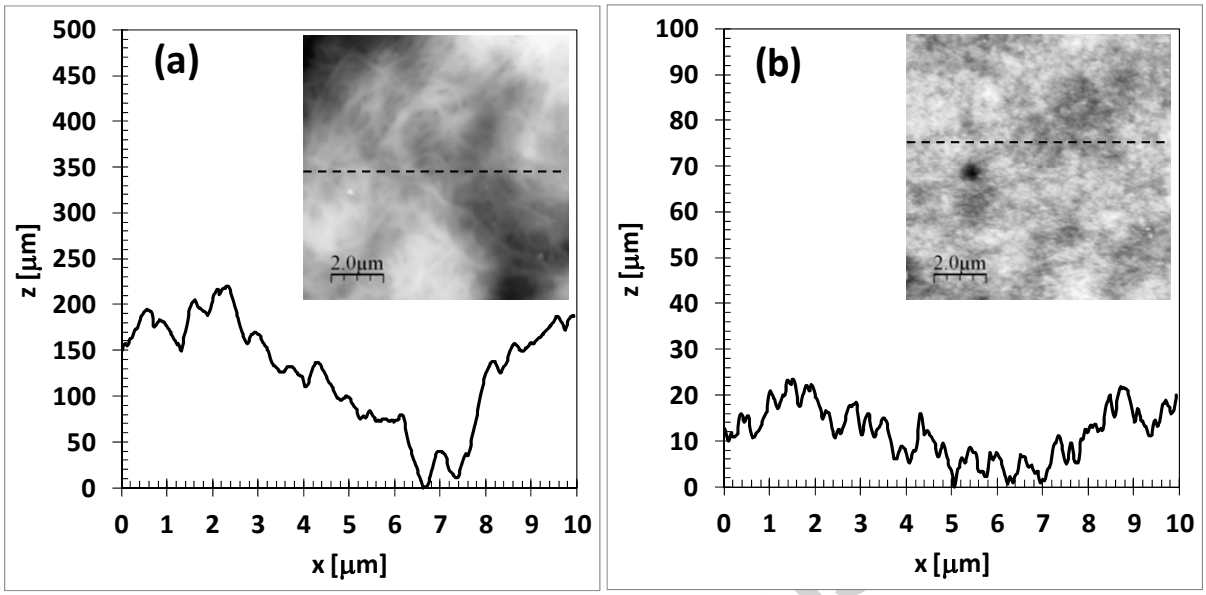

Figure 3. As shown in

Table **2**, the surface topography clearly indicates the BPs have a much rougher surface compare to the PSf supports. The BPs were found to be much rougher (34.6 nm) than the PSf supports (4.1 nm). This is explained by the fact that the diameter of the individual CNTs, investigated by transmission electron microscopy in our previous work, was found to be 20 nm [38] and that bundles of 2 or 3 entangled CNTs may exist despite following the thorough dispersion and suspension protocol described in [55].

SEM images of the surface and cross-section of both the BP and PSf supports are shown in Figure 4. The surface of the BPs was found to be an open network of entangled CNTs (Figure 4 a). The pore size distribution of the PSf and BP supports was shown to be very similar with a semi-Gaussian distribution around ~20 and 25 nm respectively (Figure 5). On the other hand, the pores of the PSf supports appeared as individual pores within a smooth, flat surface (Figure 4 b). The cross-sectional images for the BPs and PSf supports are shown in Figure 4 c and d, respectively. The porosity distribution appears to be much more homogeneous within the BPs than the PSf supports. The porosity of the BPs was previously reported to be approximately 90 % [37] with an average pore size of approximately 25 nm, distributed between 20 and 50 nm. The pore size distribution of the PSf supports was asymmetric across the thickness of the membrane, with the smallest pore size (≈ 20 nm in diameter) at the top surface where IP is performed. Figure 4d was used to analyze the porosity as a function of the membrane thickness image analysis and the ratios of dark and white areas. The asymmetric distribution is demonstrated in Figure 6 with the porosity increasing from ≈ 15 % to 60 %. The initial low porosity of the PSf support may pose significant resistance to mass transport and reduce the permeation. As demonstrated in previous studies, the porosity of the BP was even across its thickness [56] producing a membrane of uniformly high porosity which favors water permeation. In addition, the similar pore size of the PSf and BP supports means that the PA layer will be self-supporting over similar distances (size of the pore), which should allow the BP to provide sufficient support to prevent the PA layer from tearing when under pressure.

The salt mass transfer coefficient through the two membrane supports is shown in Table 1. Due to the large pore sizes of both membranes compared to salt ions, no

molecular resistances to salt permeation were assumed and direct bridging and salt diffusion occurred. The BPs exhibited a mass transfer coefficient double of that of the PSf support. Without the dense PA layer, the membrane, due to its pore size ranging between 20 to 25 nm, is therefore behaving like an ultra-filtration membrane where the mass transfer coefficient of the salt (B) may be expressed as:

$$B = \frac{D\varepsilon}{l\tau} = \frac{D}{S} \quad (4)$$

Where D is the diffusion coefficient of NaCl and the S parameter is a property of the support structure which is proportional to the thickness (*l*) and the tortuosity (τ) and inversely proportional to the porosity of the support (ε). The S parameter provides the length scale of the concentration polarization in the support layer, which is analogous to the boundary layer thickness in the external concentration polarization. Therefore, a larger S value will lead to a higher ICP [17]. Using the mass transfer data from Table 1, BPs exhibited an S value of 0.6 mm, which is less than half of that calculated for the PSf support, exhibiting an S value of 1.3 mm, and compares well with previously published S values for commercial membranes (Table 1). The S value for BPs was less than half of that calculated for the PSf support, which exhibited an S value of 1.3 mm. This indicates that the BP support should offer a lower ICP and be a much suitable supporting layer for osmotically driven processes such as FO (see Table 1). A potential concern for their use as RO support material is the mechanical strength of the BPs, as compression of the very porous BP is likely to occur at high trans-membrane pressure [35]. However, this may not be a significant issue if the tortuosity of the BP is close to 1 [57], as compression will reduce the S value while maintaining the pore size, potentially leading to increased mass transfer coefficient as demonstrated with compressed membrane distillation membranes [62].

3.2 Membrane supports with aromatic poly(amide) film

IP of a thin PA film was performed on top of the plasma exposed BP and PSf supports. Controls were performed with non-plasma treated BPs and PSf supports as well as with 20 nm pore size PTFE membranes to assess the impact of hydrophobicity on the formation of the thin film. As expected [14, 31], the stability of the IP layer on the PTFE hydrophobic supports was very low and delamination of the PA layer occurred very rapidly. This was attributed to the inability of the MPD aqueous solution to wet the surface pores of the hydrophobic support which prevents the PA layer from forming properly and adhering onto the support

As shown in Figure 2 b, the maximum water adsorption at any RH decreased with increasing average contact angle on each support. The low contact angle supports were found more stable, and this clearly shows that highly hydrophilic surfaces should be preferred for the preparation of FO membranes by IP. The data obtained at RH 80% show that the plasma treated CNT BPs exhibit higher water uptake than the PSf supports and slightly lower but nevertheless similar to the PA layer. This is interesting as this will reduce the change in water activity between the support and PA layers and may be preferential for water transport and possibly decrease the water resistance at the CNT BP-PA interface. It is also likely that the water vapour adsorption / desorption behaviors for both types of support, PSf and CNT BP, do largely differ. Water vapour is very likely to be absorbed by PSf co-polymers and cause swelling of the structure [31, 58, 59] while only adsorption should occur in the case of the CNTs due to the inability of water to penetrate the crystalline graphene network [60]. Although strong swelling and permanent structural parameters changes of CNT BPs was reported in the case of immersion/drying in alcohol mixtures [61], it is highly unlikely in the case of water due to the hydrophobic nature of the CNTs [45]. Recent work on the use of functionalized CNTs as RH detectors did not present any swelling [62] and the BP structure therefore appears as very stable to water. The enhanced adsorption of the functionalized CNT BPs is generated by the presence of hydrophilic groups on the surface of the graphene sheets composing the tubes and not by absorption within the support material as it is the case for commonly used polymeric supports. This consequently reduces the risks of ageing and degradation by consecutive swelling/drying cycles which are issues that

have been reported in the literature [14, 63]. In addition, the larger water uptake of the non-plasma treated CNTs at very high RH contents (> 80%) can be attributed to capillary condensation between the CNTs in the BP [64, 65]. This capillary action may be caused by the highly porous structure of the BPs.

In addition, SEMs of the interfacially polymerized membranes and of one commercial membrane (BW30LE) are shown in Figure 7. The film on top of the CNT BP is found to be thin and relatively smooth as CNTs could still be seen through the PA layer by transparency. This indicates, given the diameter of the CNTs (~20-25 nm [45]) that the film should not exceed ~100 nm of thickness, therefore being similar to that typically reported on PSf supports [31]. As expected from the AFM data presented in Figure 8 and values reported in the literature, the roughness on the PSf-based

membranes (Figure 7 b and Figure 8 b) was close to that of the commercial membranes

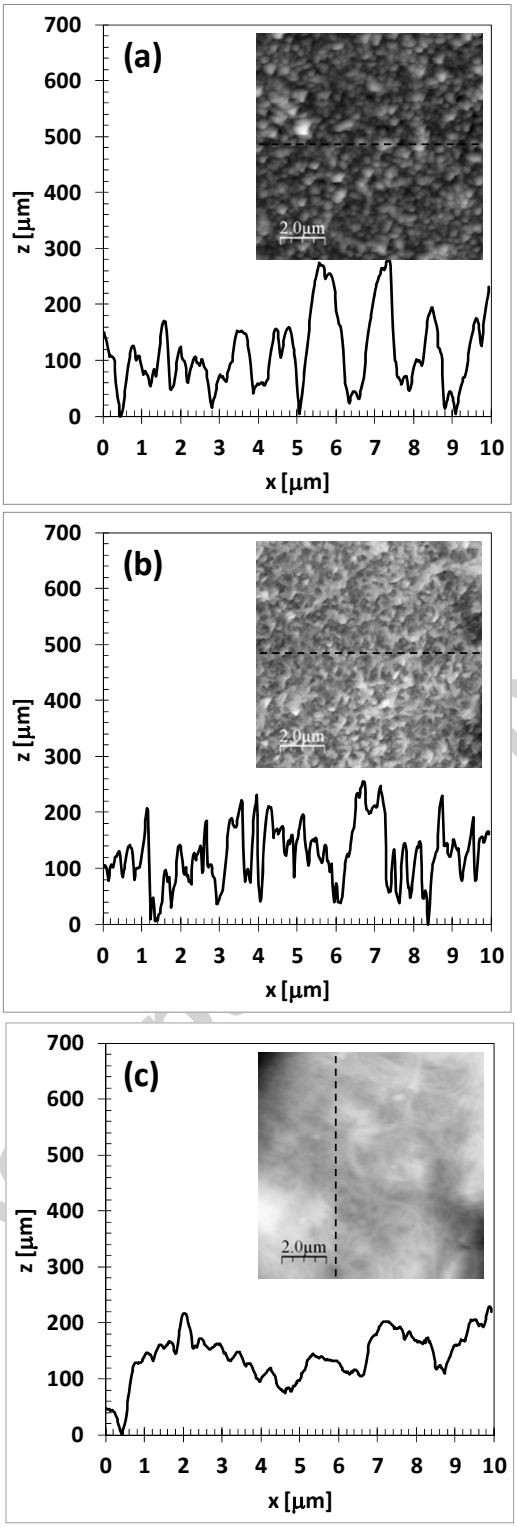

(Figure 7 a and

Figure 8 a) with an average roughness value of 49.7 nm for the commercial membranes as opposed to 56 nm for the PSf supported PA membrane (

Table 2). The surface morphology was very different to the aromatic PA deposited on the BPs (Figure 7c and Figure 8 c), which appears to be a smoother surface (roughness of only 29.2 nm as shown in

Table 2). The roughness and geometry of the supporting layer surface was therefore, demonstrated to highly affect the morphology of the PA layer. It is also interesting to note that the most hydrophilic surface lead to the most stable and smoothest PA deposition. This follows trends previously reported in [31], where PSf supports used for the preparation of RO membranes, were chemically modified to vary their degree of hydrophilicity prior to performing IP. The water meniscus orientation at the surface of the pores will therefore dictate the stability and penetration depth of the PA layer within the support. Furthermore, given the IP procedure that was followed in our work, it is also likely that the vacuum applied during the polymerization further enhanced the penetration of PA within the top of the CNT BP. This might also have improved the adhesion of the PA layer by partially embedding it into the support, across the thickness of a few CNTs.

Finally, the salt mass transfer coefficient through TFC membranes made using different supports is tabulated in Table 3. It can be seen that the salt mass transfer coefficient related to the PA-BP membranes was actually lower by ≈ 15 % to those of the commercial membranes. In fact, hydrophilic supports used for IP were shown [31] to produce thinner, smoother and slightly less permeable membranes due to the larger penetration of PA within the membrane pores. This is well correlated with our results as the CNT BP-PA membranes exhibited lower salt permeability than the PSf support membranes, although the thickness of the PA was likely to be very similar. This result is highly promising as it demonstrates that membranes fabricated on more exotic supports can also be competitive in FO. The salt diffusion tests were performed over 6-8 h and no failures were reported for the tested samples. This clearly demonstrates that IP can be successfully performed on top of the nano-structured supports, such as BPs, and could lead to membranes exhibiting lower resistance to water permeation in FO while presenting improved salt rejection when compared to commercially available TFC membranes. In addition, the large scope of possible functional groups that can be grafted onto CNTs outer walls [36, 60] opens highly promising prospects for CNTs to be used and integrated into membrane support materials.

A number of other hydrophilic, high porosity and lower processing costs materials would also make good candidates as support structures for osmotically driven membranes, including highly porous structures made of metal oxide nanotubes [66], metal foams [67, 68] or aerogels [69, 70].

4. Conclusion

It was demonstrated that highly hydrophilic supports were more suitable for the processing of stable membranes for salt diffusion membranes for use in applications such as FO. CNT BPs especially have a strong potential to be used as a support for TFC membranes. The large porosity of the BPs, added to their even structure and strong chemical resistance make them promising supports for high flux TFC membranes. Their chemistry can be finely tuned to enhance their water adsorption and therefore facilitate transport. In addition, they can be processed in very thin sheets that can further enhance water permeation and reduce salt permeation when compared to commercial PSf supports. Furthermore the surface energy and roughness of the support were shown to influence the formation of smooth films by interfacial polymerization. CNTs offer fascinating prospects as the tubes can be pre-functionalized with groups showing greater affinity for PA, or with some of the monomers used in its interfacial polymerization, which could lead to improved polymerization patterns and ultimately lower the thickness of the active layer. One major limitation for the use of BPs as RO supports might however resides in their high compressibility, potentially reducing the effective porosity at large trans-membrane pressure difference. Solutions to improve the mechanical stability could lie in adding extra supporting layers, such as a poly(amide) mesh or metal grid and further work is required to fully perceive the potential of these novel types of supports. This work has explored the concept of the novel material, but clearly more work is needed when fixed on a particular application (eg. RO or FO) to extract the practical performance in terms of salt rejection and water flux.

Acknowledgement

The authors would like to thank Prof. Sandra Kentish for fruitful discussions and for providing moral support to the scope of this work as well as Dr. Colin Scholes for his advice on the VTI measurements, as well as Dr. Yen Truong for advice on the PMI

porometer tests. The authors also thank the Particulate Fluid Processing Center at the University of Melbourne for supporting this work. Dow Filmtec for supplying the BW30 RO membrane samples and GE Water Technologies for supplying the PSf support material.

Figures and tables

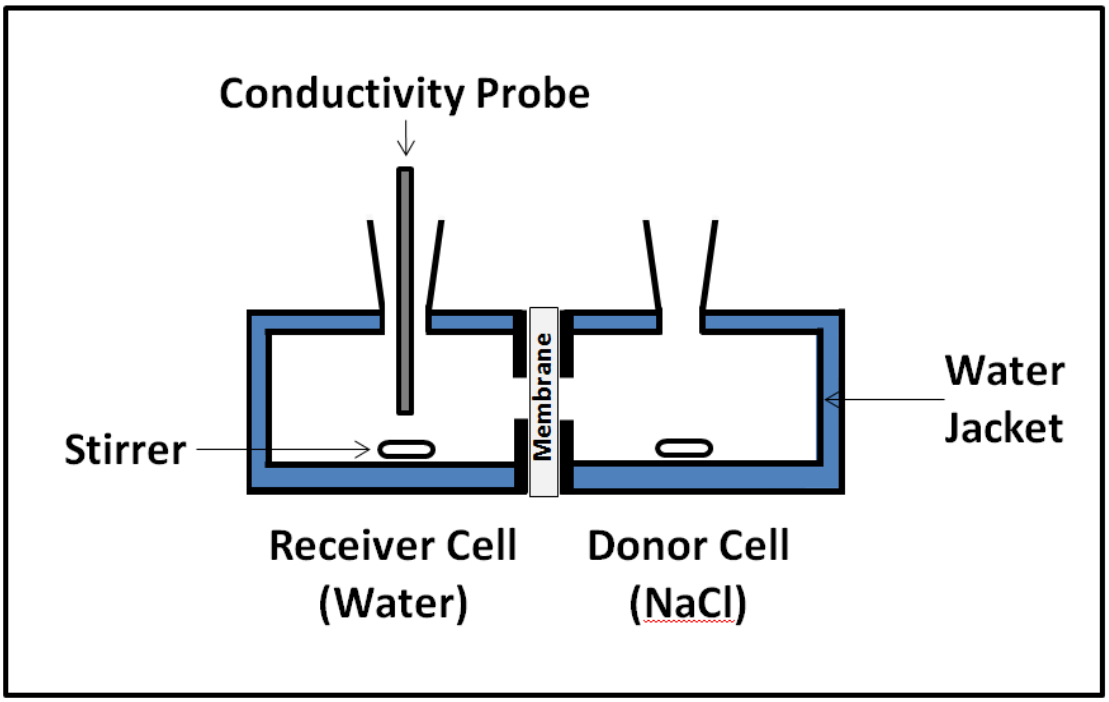

Figure 1 Schematic of the stirred cells and position of the probes.

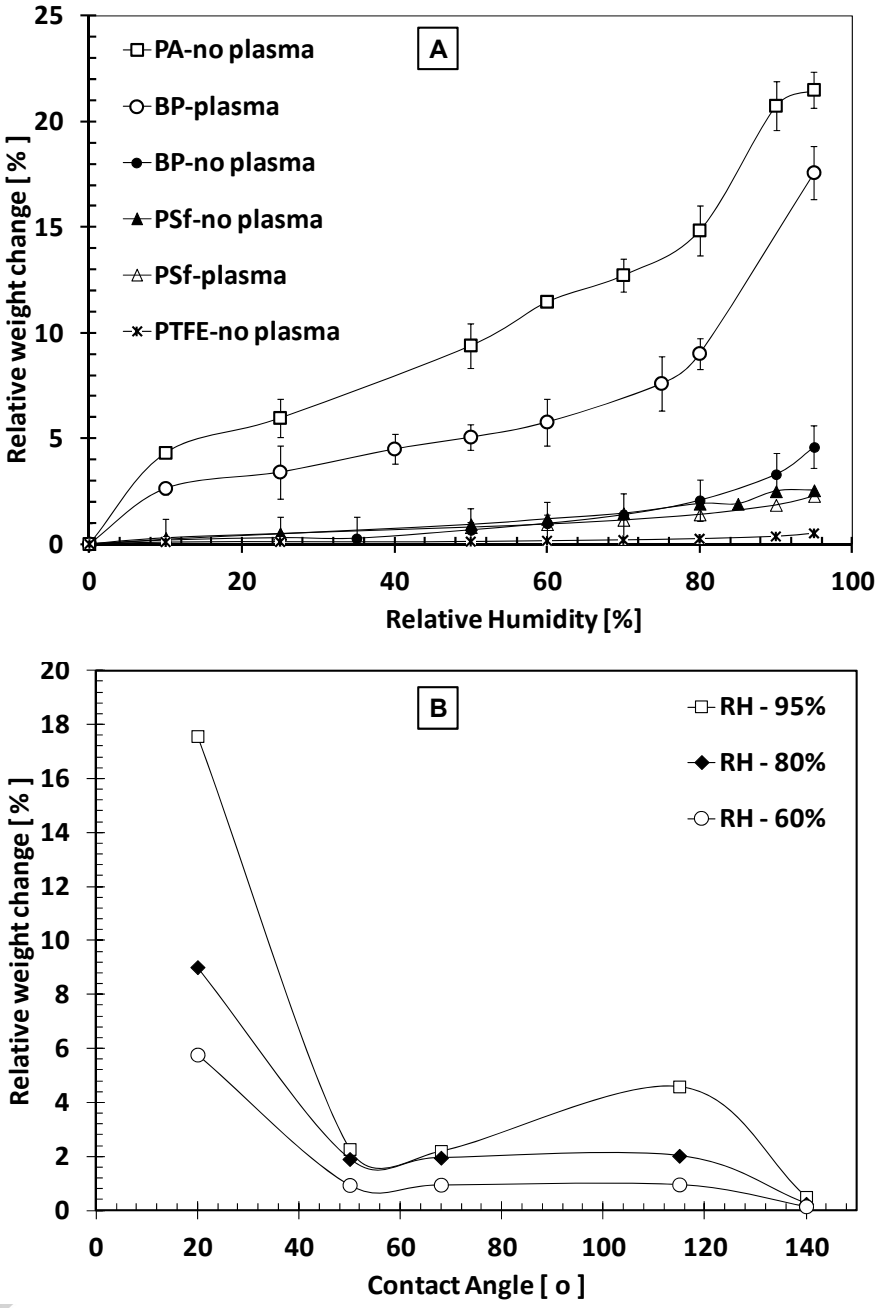

Figure 2: (A) The percentage of water vapour uptake at different RH for PA top layer only, plasma treated BP, BP without plasma treatment, PSf support without plasma, PSf with plasma, and Teflon without plasma; (B) Relative water adsorption changes as a function of the surface contact angle of the supports.

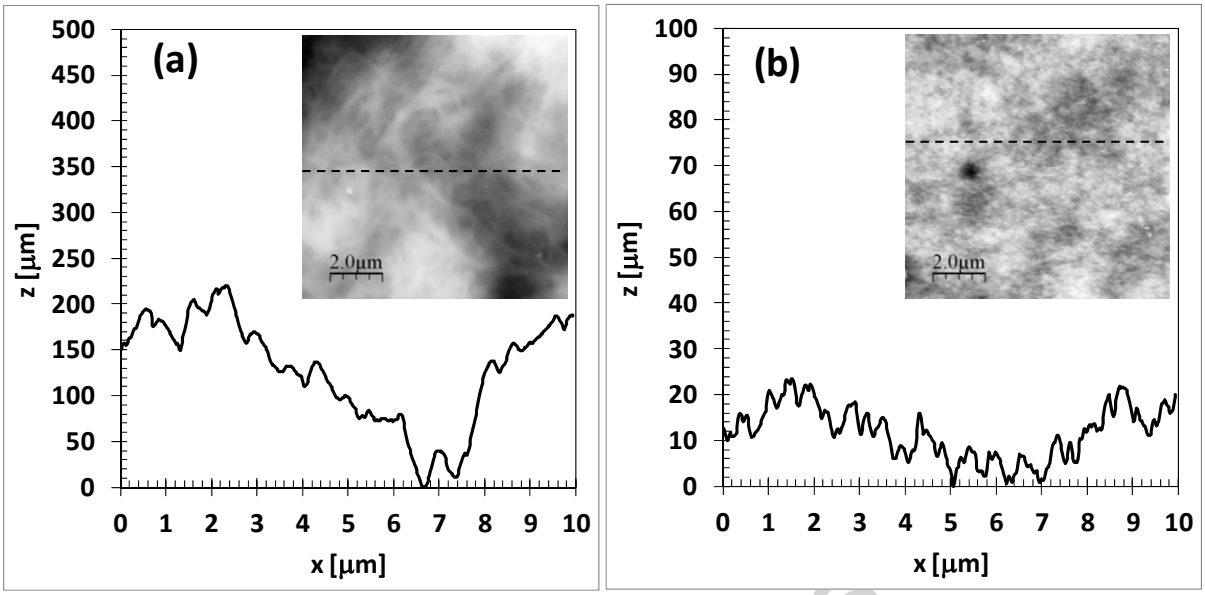

Figure 3: AFM images of the surface (insert) and surface topography of supports without PA interfacial polymerisation: (a) BP and (b) PSf support layer. The dotted line indicates where the surface topography was mapped.

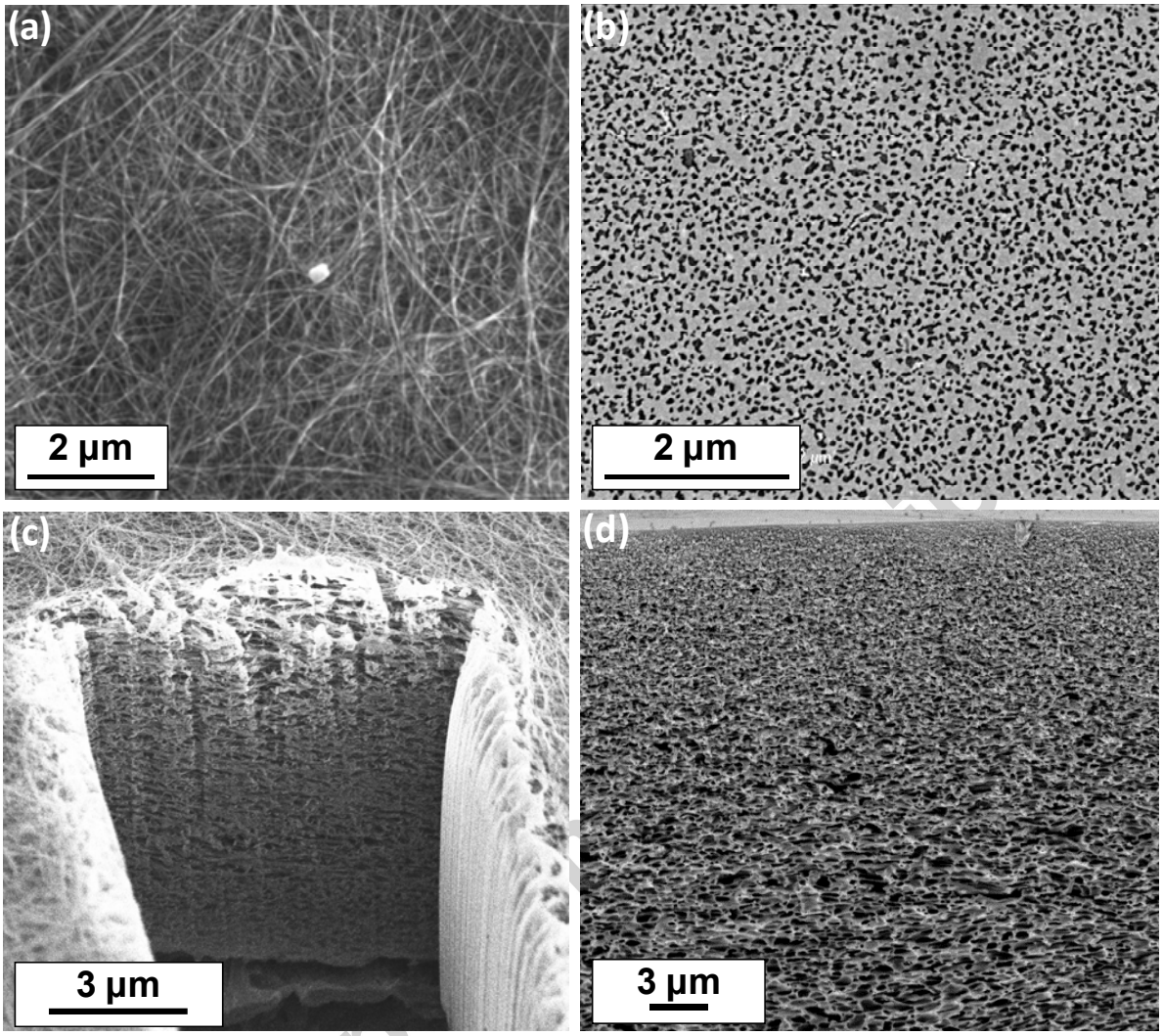

Figure 4: SEM images of the surface of (a) BP and (b) PSf, and the cross-section of (c) BP and (d) PSf.

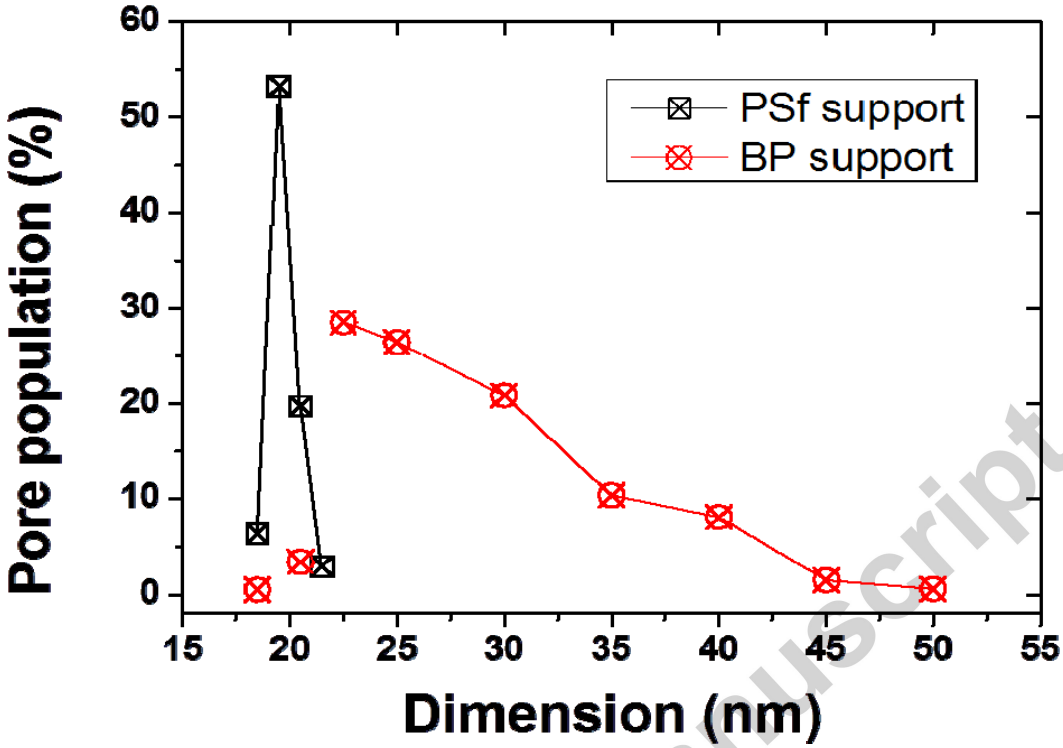

Figure 5 Pore size distribution of both PSf and BP supports.

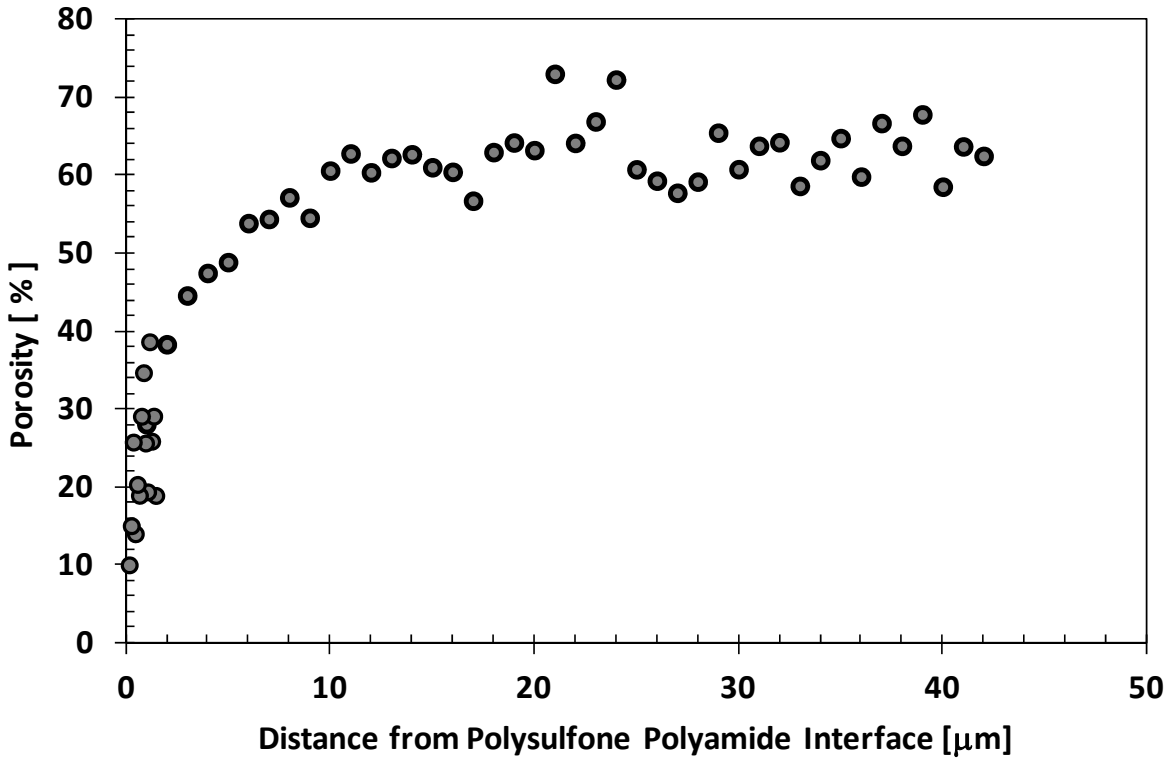

Figure 6: Porosity as a function of distance away from the top PSf surface.

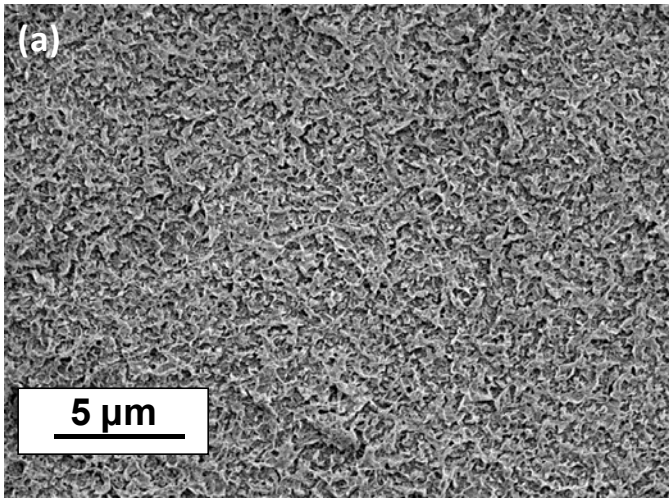

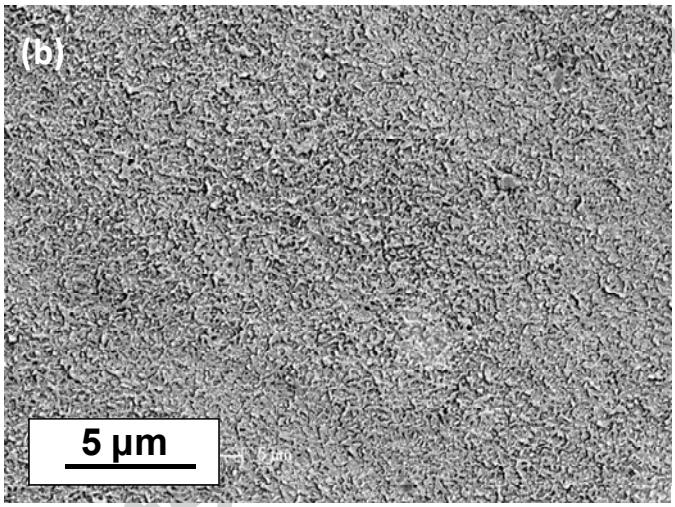

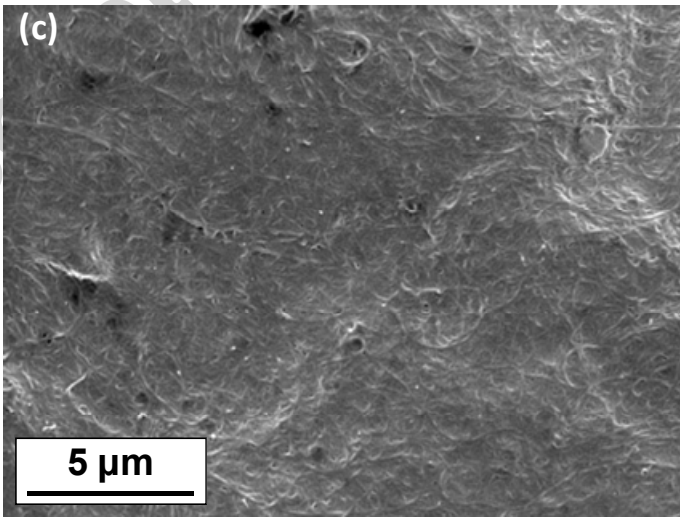

Figure 7: SEM images of the aromatic polyamide surface formed on the membrane supports via IP (a) commercial BW30LE, (b) PSf support and (c) BP support.

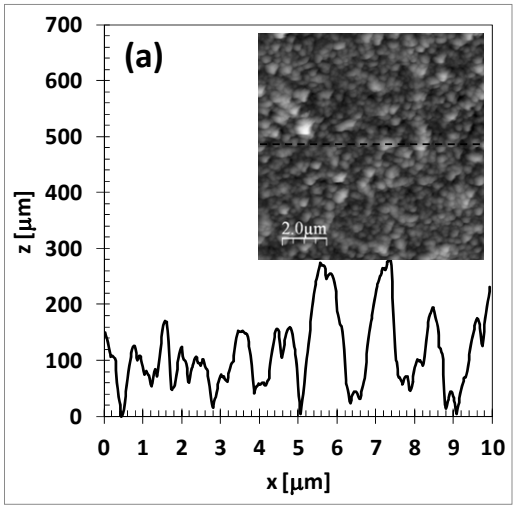

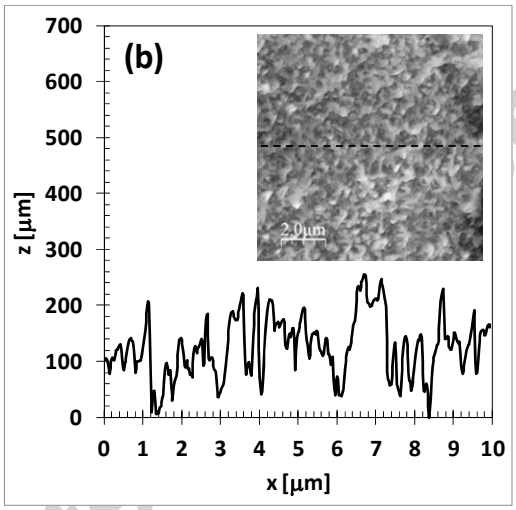

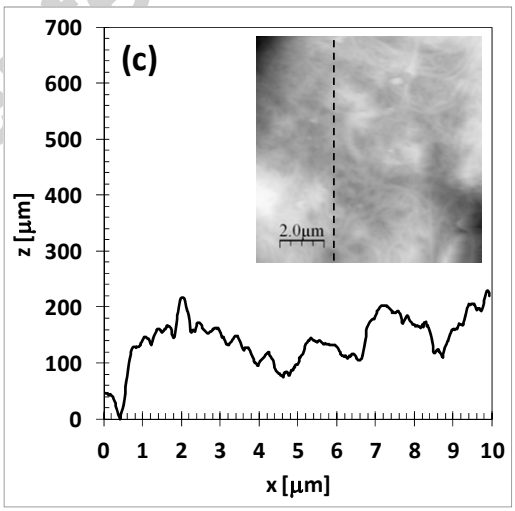

Figure 8: AFM images of the surface (insert) and surface topography of polyamides on: (a) BW30L, (b) PSf support and (c) TFC BP membrane. The dotted line indicates where the surface topography was mapped.

Table 1: Characteristics of the membrane supports tested in this study and of values taken from the literature for commercial HTI membranes. The contact angle on the plasma exposed CNTs was so low that an accurate measurement was difficult and an upper bound of 25^{o}.

	BP support untreated	**BP support plasma treated**	**PSf support untreated**	**PSf support plasma treated**	**HTI support**	**PTFE Pall 20 nm support**
Contact angle (^{o})	115 ± 3	< 20 ± 5	68 ± 2	50 ±5	66.4 ± 1.3 [8]	140 ± 2
Water uptake at 95 % relative humidity (wt%)	5.7	17.6	2.2	2.27	-	0.5
Thickness (μm)	-	12.3 ± 1.5	43 ± 3	-	-	-
Salt permeability (10^{-4} cm.s^{-1})	-	2.6	1.24	-	-	-
S (mm)	-	0.62	1.3	-	0.7 – 1.4 [8]	-

Table 2: AFM roughness on the surface of the supports and TFC membranes (nm).

	RMS (2.5 µm × 2.5 µm)
BP alone	34.6 ± 2.2
PSf alone	4.1 ± 0.3
BW30LE	49.7 ± 5.2
PA-PSf	56.0 ± 4.8
PA-BP	29.2 ± 3.7

Table 3: Salt mass transfer coefficient through TFC membranes from commercially available BW30LE, membrane synthesised in the laboratory using PSf and membrane made using BP support.

	Salt permeability (10^{-5} cm.s^{-1})
BW30LE	1.5 ± 0.12
PA-PSf	1.71 ± 0.13
PA-BP	1.28 ± 0.36

References

[1] L.F. Greenlee, D.F. Lawler, B.D. Freeman, B. Marrot, P. Moulin, Reverse osmosis desalination: Water sources, technology, and today's challenges, Water Research, 43 (2009) 2317-2348.
[2] K.P. Lee, T.C. Arnot, D. Mattia, A review of reverse osmosis membrane materials for desalination—Development to date and future potential, Journal of Membrane Science, 370 (2011) 1-22.
[3] T. Sankai, G. Ding, N. Emori, S. Kitamura, K. Katada, A. Koshio, T. Maruyama, K. Kudo, Y. Inamori, Treatment of domestic wastewater mixed with crushed garbage and garbage washing water by advanced Gappei-Shori Johkaso, Water Science and Technology, 36 (1997) 175-182.
[4] T.Y. Cath, A.E. Childress, M. Elimelech, Forward osmosis: principles, applications, and recent developments, J. Membr. Sci., 281 (2006) 70-87.
[5] M. Ernst, A. Bismarck, J. Springer, M. Jekel, Zeta-potential and rejection rates of a polyethersulfone nanofiltration membrane in single salt solutions, Journal of Membrane Science, 165 (2000) 251-259.
[6] S. Zhao, L. Zou, D. Mulcahy, Brackish water desalination by a hybrid forward osmosis–nanofiltration system using divalent draw solute, Desalination, 284 (2012) 175-181.
[7] Y. Zhao, Q. Yuan, A comparison of nanofiltration with aqueous and organic solvents, Journal of Membrane Science, 279 (2006) 453-458.
[8] S. Zhao, L. Zou, Effects of working temperature on separation performance, membrane scaling and cleaning in forward osmosis desalination, Desalination, 278 (2011) 157-164.
[9] R.E. Kravath, J.A. Davis, Desalination of sea water by direct osmosis, Desalination, 16 (1975) 151-155.
[10] J.O. Kessler, C.D. Moody, Drinking water from sea water by forward osmosis, Desalination, 18 (1976) 297-306.
[11] McCutcheon, M. Elimelech, Forward (direct) osmosis desailination using polymeric membranes, Abstracts of papers - American Chemical Society, 228 (2004) U633-U633.
[12] H.Y. Ng, W. Tang, W.S. Wong, Performance of Forward (Direct) Osmosis Process: Membrane Structure and Transport Phenomenon, Environmental Science & Technology, 40 (2006) 2408-2413.
[13] M. Mulder, Basic principles of membrane technology, 1996.
[14] J.T. Arena, B. McCloskey, B.D. Freeman, J.R. McCutcheon, Surface modification of thin film composite membrane support layers with polydopamine: Enabling use of reverse osmosis membranes in pressure retarded osmosis, Journal of Membrane Science, 375 (2011) 55-62.
[15] D.R. Paul, Reformulation of the solution-diffusion theory of reverse osmosis, Journal of Membrane Science, 241 (2004) 371-386.
[16] G. Jonsson, Methods for determining the selectivity of reverse osmosis membranes, Desalination, 24 (1978) 19-37.
[17] G. Jonsson, The influence of the porous sublayer on the salt rejection and reflection coefficient of asymmetric CA membranes, Desalination, 34 (1980) 141-157.
[18] N.Y. Yip, A. Tiraferri, W.A. Phillip, J.D. Schiffman, M. Elimelech, High Performance Thin-Film Composite Forward Osmosis Membrane, Environmental Science and Technology, 44 (2010) 3812-3818.
[19] W.C.L. Lay, J. Zhang, C. Tang, R. Wang, Y. Liu, A.G. Fane, Factors affecting flux performance of forward osmosis systems, Journal of Membrane Science.
[20] B. Van der Bruggen, J. Schaep, D. Wilms, C. Vandecasteele, Influence of molecular size, polarity and charge on the retention of organic molecules by nanofiltration, Journal of Membrane Science, 156 (1999) 29-41.
[21] S. Zhao, L. Zou, Relating solution physicochemical properties to internal concentration polarization in forward osmosis, Journal of Membrane Science, 379 (2011) 459-467.
[22] G.D. Mehta, S. Loeb, Internal polarization in the porous substructure of a semipermeable membrane under pressure-retarded osmosis, Journal of Membrane Science, 4 (1978) 261-265.
[23] G.D. Mehta, S. Loeb, Performance of permasep B-9 and B-10 membranes in various osmotic regions and at high osmotic pressures, Journal of Membrane Science, 4 (1978) 335-349.

[24] N.Y. Yip, A. Tiraferri, W.A. Phillip, J.D. Schiffman, M. Elimelech, High performance thin-film composite forward osmosis membrane, Environ. Sci. Technol., 44 (2010) 3812-3818.
[25] J.R. McCutcheon, M. Elimelech, Influence of membrane support layer hydrophobicity on water flux in osmotically driven membrane processes, J. Membr. Sci., 318 (2008) 458-466.
[26] R.L. Mcginnis, Spiral Wound Membrane Module for Forward Osmotic Use, in, Yale University (New Haven, CT, US), United States 2011.
[27] G. Guillen, E.M.V. Hoek, Modeling the impacts of feed spacer geometry on reverse osmosis and nanofiltration processes, Chemical Engineering Journal (Lausanne), 149 (2009) 221-231.
[28] K.L. Lee, R.W. Baker, H.K. Lonsdale, Membranes for power-generation by pressure-retarded osmosis, J. Membr. Sci., 8 (1981) 141-171.
[29] N. Misdan, W.J. Lau, A.F. Ismail, Seawater Reverse Osmosis (SWRO) desalination by thin-film composite membrane—Current development, challenges and future prospects, Desalination.
[30] S. Zhao, L. Zou, C.Y. Tang, D. Mulcahy, Recent developments in forward osmosis: Opportunities and challenges, Journal of Membrane Science, 396 (2012) 1-21.
[31] A.K. Ghosh, E.M.V. Hoek, Impacts of support membrane structure and chemistry on polyamide–polysulfone interfacial composite membranes, Journal of Membrane Science, 336 (2009) 140-148.
[32] Q. Yang, K.Y. Wang, T.-S. Chung, A novel dual-layer forward osmosis membrane for protein enrichment and concentration, Separation and Purification Technology, 69 (2009) 269-274.
[33] J. Zhang, W. Liu, Thin porous metal sheet-supported NaA zeolite membrane for water/ethanol separation, Journal of Membrane Science, 371 (2011) 197-210.
[34] X. Song, Z. Liu, D.D. Sun, Nano Gives the Answer: Breaking the Bottleneck of Internal Concentration Polarization with a Nanofiber Composite Forward Osmosis Membrane for a High Water Production Rate, Advanced Materials, 23 (2011) 3256-3260.
[35] R.L.D. Whitby, S.V. Mikhalovsky, V.M. Gun'ko, Mechanical performance of highly compressible multi-walled carbon nanotube columns with hyperboloid geometries, Carbon, 48 (2010) 145-152.
[36] Z. Spitalsky, D. Tasis, K. Papagelis, C. Galiotis, Carbon nanotube-polymer composites: Chemistry, processing, mechanical and electrical properties, Progress in Polymer Science, 35 (2010) 357-401.
[37] L. Dumée, K. Sears, J. Schült, N. Finn, C. Huynh, S. Hawkins, M. Duke, S. Gray, Characterization and evaluation of carbon nanotube bucky-paper membranes for direct contact membrane distillation, J. Membr. Sci., 351 (2010) 36-43.
[38] L.F. Dumée, K. Sears, J. Schütz, N. Finn, C. Huynh, S. Hawkins, M. Duke, S. Gray, Characterization and evaluation of carbon nanotube Bucky-Paper membranes for direct contact membrane distillation, Journal of Membrane Science, 351 (2010) 36-43.
[39] M. Yu, H.H. Funke, J.L. Falconer, R.D. Noble, High Density, Vertically-Aligned Carbon Nanotube Membranes, Nano Lett., 9 (2008) 225-229.
[40] M. Kim, Y.-B. Park, O.I. Okoli, C. Zhang, Processing, characterization, and modeling of carbon nanotube-reinforced multiscale composites, Composites Science and Technology, 69 (2009) 335-342.
[41] M. Endo, T. Hayashi, Y. Ahm Kim, M. Terrones, M.S. Dresselhaus, Applications of carbon nanotubes in the twenty–first century, Philosophical Transactions of the Royal Society of London. Series A: Mathematical, Physical and Engineering Sciences, 362 (2004) 2223-2238.
[42] Y. Li, M. Kröger, A theoretical evaluation of the effects of carbon nanotube entanglement and bundling on the structural and mechanical properties of buckypaper, Carbon, 50 (2012) 1793-1806.
[43] A. Deneuve, K. Wang, I. Janowska, K. Chizari, D. Edouard, O. Ersen, M.-J. Ledoux, C. Pham-Huu, Bucky paper with improved mechanical stability made from vertically aligned carbon nanotubes for desulfurization process, Applied Catalysis A: General, 400 (2011) 230-237.
[44] K. Sears, L. Dumée, J. Schütz, M. She, C. Huynh, S. Hawkins, M. Duke, S. Gray, Recent Developments in Carbon Nanotube Membranes for Water Purification and Gas Separation, Materials, 3 (2010) 127-149.
[45] L. Dumée, V. Germain, K. Sears, J. Schütz, N. Finn, M. Duke, S. Cerneaux, D. Cornu, S. Gray, Enhanced durability and hydrophobicity of carbon nanotube bucky paper membranes in membrane distillation, Journal of Membrane Science, 376 (2011) 241-246.

[46] L. Dumée, K. Sears, J. Schütz, N. Finn, M. Duke, S. Gray, Carbon nanotube based composite membranes for water desalination by membrane distillation, Desalination and water treatment, 17 (2010) 7.
[47] L. Chen, H. Xie, Y. Li, W. Yu, Carbon nanotubes with hydrophilic surfaces produced by a wet-mechanochemical reaction with potassium hydroxide using ethanol as solvent, Materials Letters, 63 (2009) 45-47.
[48] A. Villa, M. Plebani, M. Schiavoni, C. Milone, E. Piperopoulos, S. Galvagno, L. Prati, Tuning hydrophilic properties of carbon nanotubes: A challenge for enhancing selectivity in Pd catalyzed alcohol oxidation, Catalysis Today.
[49] C.P. Huynh, S.C. Hawkins, Understanding the synthesis of directly spinnable carbon nanotube forests, Carbon, 48 (2010) 1105-1115.
[50] L. Dumee, M.R. Hill, M. Duke, L. Velleman, K. Sears, J. Schutz, N. Finn, S. Gray, Activation of gold decorated carbon nanotube hybrids for targeted gas adsorption and enhanced catalytic oxidation, Journal of Materials Chemistry, 22 (2012) 9374-9378.
[51] G.Q. Chen, C.A. Scholes, G.G. Qiao, S. Kentish, Watervapor permeation in polyimide membranes, J. Membr. Sci., 379 (2011) 479-487.
[52] W. Jost, Diffusion in solids, liquids and gases, Academic Press, New York, 1960.
[53] V. Chirila, G. Marginean, W. Brandl, Effect of the oxygen plasma treatment parameters on the carbon nanotubes surface properties, Surface and Coatings Technology, 200 (2005) 548-551.
[54] C. Chen, A. Ogino, X. Wang, M. Nagatsu, Plasma treatment of multiwall carbon nanotubes for dispersion improvement in water, Applied Physics Letters, 96 (2010) 131504-131503.
[55] L. Dumée, J.L. Campbell, K. Sears, J. Schütz, N. Finn, M. Duke, S. Gray, The impact of hydrophobic coating on the performance of carbon nanotube bucky-paper membranes in membrane distillation, Desalination, In Press, Corrected Proof.
[56] L. Dumee, L. Velleman, K. Sears, M. Hill, J. Schutz, N. Finn, M. Duke, S. Gray, Control of Porosity and Pore Size of Metal Reinforced Carbon Nanotube Membranes, Membranes, 1 (2010) 25-36.
[57] Y. Li, M. Kröger, Computational study on entanglement length and pore size of carbon nanotube buckypaper, Applied Physics Letters, 100 (2012) 021907.
[58] K.A. Schult, D.R. Paul, Water sorption and transport in a series of polysulfones, Journal of Polymer Science Part B: Polymer Physics, 34 (1996) 2805-2817.
[59] A.K. Ghosh, B.-H. Jeong, X. Huang, E.M.V. Hoek, Impacts of reaction and curing conditions on polyamide composite reverse osmosis membrane properties, Journal of Membrane Science, 311 (2008) 34-45.
[60] D. Tasis, N. Tagmatarchis, A. Bianco, M. Prato, Chemistry of Carbon Nanotubes, Chemical Reviews, 106 (2006) 1105-1136.
[61] R.L.D. Whitby, T. Fukuda, T. Maekawa, S.L. James, S.V. Mikhalovsky, Geometric control and tuneable pore size distribution of buckypaper and buckydiscs, Carbon, 46 (2008) 949-956.
[62] J.T.W. Yeow, J.P.M. She, Carbon nanotube-enhanced capillary condensation for a capacitive humidity sensor, Nanotechnology, 17 (2006) 5441.
[63] R.F. Eaton, R.J. Roe, G.L. Wilkes, A.V. Tobolsky, Thermodynamics of Hydrophilic Polymer Membranes: The Degree of Swelling and Salt Partition Coefficient, in: D.o.O.C.a.P.C. American Chemical Society (Ed.), 1975, pp. pp. 503–508.
[64] A. Grosman, C. Ortega, Capillary Condensation in Porous Materials. Hysteresis and Interaction Mechanism without Pore Blocking/Percolation Process, Langmuir, 24 (2008) 3977-3986.
[65] V.V. Yaminsky, The hydrophobic force: the constant volume capillary approximation, Colloids and Surfaces A: Physicochemical and Engineering Aspects, 159 (1999) 181-195.
[66] D.-Y. Kang, J. Zang, C.W. Jones, S. Nair, Single-Walled Aluminosilicate Nanotubes with Organic-Modified Interiors, The Journal of Physical Chemistry C, 115 (2011) 7676-7685.
[67] B.C. Tappan, S.A. Steiner, E.P. Luther, Nanoporous Metal Foams, Angewandte Chemie International Edition, 49 (2010) 4544-4565.
[68] J. Banhart, Manufacture, characterisation and application of cellular metals and metal foams, Prog. Mater. Sci., 46 (2001) 559-U553.

[69] J. Wang, M. Chen, C. Wang, J. Wang, J. Zheng, A facile method to prepare carbon aerogels from amphiphilic carbon material, Materials Letters, 68 (2012) 446-449.
[70] T.-P. Fellinger, R.J. White, M.-M. Titirici, M. Antonietti, Borax-Mediated Formation of Carbon Aerogels from Glucose, Advanced Functional Materials, (2012) n/a-n/a.

- Investigating new supports for the preparation of forward osmosis membranes
- Testing the impact of hydrophillicity of support materials on the stability of interfacially polymerized films to delaminating
- Characterizing and testing the salt permeation of the composite nanotube – poly(amide) membranes